Chemical Geology 254 (2008) 73-86

Contents lists available at ScienceDirect

Chemical Geology

journal homepage: www.elsevier.com/locate/chemgeo

Jarosite dissolution II—Reaction kinetics, stoichiometry and acid flux

Susan A. Welch [a,c,*,1,2], Dirk Kirste [a,c,3], Andrew G. Christy [a,1], Fern R. Beavis [a,c,1], Sara G. Beavis [a,b,c,1,2]

[a] Department of Earth and Marine Sciences, The Australian National University, Canberra ACT 0200, Australia
[b] Fenner School of Environment and Society, The Australian National University, Canberra ACT 0200, Australia
[c] Cooperative Research Centre for Landscape Environments and Mineral Exploration (CRC LEME), The Australian National University, Canberra ACT 0200, Australia

ARTICLE INFO

Article history:
Received 17 March 2008
Received in revised form 3 June 2008
Accepted 4 June 2008

Editor: J. Fein

Keywords:
Jarosite
Acid sulfate soils
Weathering
Mineral dissolution

ABSTRACT

A study was undertaken to characterize a natural jarosite sample from an acid sulfate soils site and to experimentally determine the kinetics of dissolution and major ion release from jarosite under a range of different conditions. The jarosite was sourced from a degraded acid sulfate soil site that displays spatio-temporal variability in acidity on the mid north coast of NSW, Australia. Dissolution reaction rates varied as a function of solution composition but were roughly proportional to the degree of undersaturation, and the reaction pathway towards saturation was complex. The short-term reaction rates (<12 days) decreased with increasing acidity, sulfate or iron. Over the longer term, there was a shift from congruent to incongruent dissolution, with precipitation of Fe–(OOH) solid, and with little further change in saturation index. The dissolution rates of the natural mineral were 1–3 orders of magnitude slower than experimentally determined reaction rates of synthetic jarosite samples run under similar experimental conditions, suggesting that residual solids were inhibiting reaction.

The slow reaction rates of this study are probably more typical of jarosite in natural acid sulfate environments than the faster dissolution of clean synthetic jarosite. However, the shift in mechanism over a few days from near-congruent dissolution producing little acidity but much mobile Fe^{3+}, to production of acidity as that Fe^{3+} precipitates, indicates that acidity can readily spread from jarosite dissolving under moderately acid conditions.

1. Introduction

Jarosite and alunite are isostructural hydrous sulfate minerals belonging to the alunite group, with a general formula of $AB_3(SO_4)_2(OH)_6$ (Fig. 1) (Ralph and Ralph, 1993; Barthelemy, 2000). The B cations have octahedral coordination and are commonly Fe^{3+} (jarosite subgroup) or Al^{3+} (alunite subgroup). Cations in the A site have coordination ≥9 and are commonly K^+, Na^+, or H_3O^+. The ideal endmember composition for jarosite *sensu strictu* is $KFe_3(SO_4)_2(OH)_6$. Jarosite and alunite minerals commonly occur in acid sulfate soils and acid mine drainage sites where pyrite has been oxidized, pH decreases below 3.7 (c.f. White et al., 1997; Bigham and Nordstrom, 2000; Jambor et al., 2000) and water is limited. Jarosite and alunite have also been described in acidic hypersaline evaporite basins in Australia such as Lake Tyrrell (Alpers et al., 1992), and in the Antarctic (Gore et al., 1996). Recently, jarosite has been detected on the surface of Mars (Klingelhöfer et al., 2004; Madden et al., 2004).

In some coastal acid sulfate soil sites in Australia jarosite is particularly important in controlling acidity because it represents a major source of acidity (cf. White et al., 1997; Tulau and Naylor, 1999; Somerville et al., 2004; Beavis et al., 2005). Remediation strategies for acid sulfate soil sites, such as flooding to prevent further oxidation of pyrite, can have disastrous results if jarosite is abundant because reaction in water releases more acid to solution (White et al., 1997) as demonstrated in Eq. (1):

$$KFe_3(SO_4)_2(OH)_6 + 3H_2O \rightarrow 3Fe(OH)_3 + K^+ + 3H^+ + 2SO_4^{2-} \quad (1)$$

Alternatively, if jarosite reacts under more acidic conditions, producing soluble ferric iron instead of ferric hydroxides, this can catalyse pyrite oxidation (Singer and Stumm, 1970):

$$FeS_2 + 14Fe^{3+} + 8H_2O \rightarrow 15Fe^{2+} + 2SO_4^{2-} + 16H^+ \quad (2)$$

The ferric iron controlled oxidation of pyrite is orders of magnitude faster than the reaction with molecular oxygen (Singer and Stumm, 1970). Consequently, in acid sulfate soil environments, jarosite dissolution kinetics and the release of dissolved ferric iron can be a major factor controlling pyrite oxidation and the generation of acidity under anoxic conditions.

Experimental studies on the formation and reactivity of these hydrous sulfate mineral phases yield variable results with respect to the stability of

* Corresponding author. Department of Earth and Marine Sciences, The Australian National University, Canberra ACT 0200, Australia. Fax: +61 2 6125 5544.
E-mail addresses: swelch@ems.anu.edu.au, welch.318@osu.edu (S.A. Welch).
[1] Research School of Earth Sciences, The Australian National University, Canberra, ACT, Australia.
[2] School of Earth Sciences, The Ohio State University, Columbus OH, 43210, USA.
[3] Department of Earth Sciences, Simon Fraser University, Burnaby, BC, Canada.

0009-2541/$ – see front matter © 2008 Elsevier B.V. All rights reserved.
doi:10.1016/j.chemgeo.2008.06.010

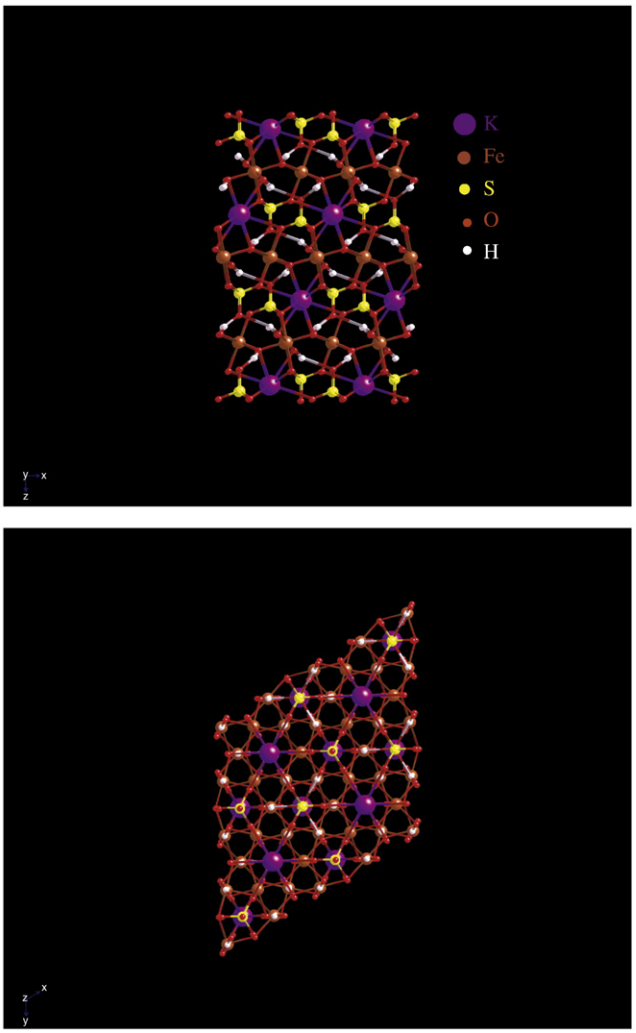

Fig. 1. Model of jarosite crystal structure showing A (K^+), B (Fe^{3+}) and tetrahedral (SO_4^{2-}) sites.

jarosite (cf. Stoffregen, 1993; Baron and Palmer, 1996 and references therein; Bigham and Nordstrom, 2000; Drouet and Navrotsky, 2003; Drouet et al., 2004). Reported values for solubility constants range over several orders of magnitude because both natural and synthetic jarosite rarely have the pure endmember composition (Bigham and Nordstrom, 2000; Dutrizac and Jambor, 2000; Papike et al 2006a, b; Smith et al., 2006b). Stability and reactivity are dependent on the degree of isomorphous substitution into the A and B sites. Na^+ or H_3O^+ substitution into the A site greatly increases jarosite reactivity and solubility. In addition to these common substitutions, other ions such as NH_4^+, Ag^+, Tl^+, Pb^{2+}, Ca^{2+}, Sr^{2+}, Ba^{2+}, Cu^{2+}, Hg^{2+}, and the REE can substitute into the A site, Cr^{3+}, V^{3+} Ga^{3+} and Cu^{2+}, can substitute into the B site, and the oxyanions CrO_4^{2-}, PO_4^{3-}, and AsO_4^{3-} can substitute for sulfate (Dutrizac and Jambor, 2000; Becker and Gasharova, 2001; Dill, 2001; Kolitsch and Pring, 2001). This is an important characteristic because it means that jarosite can act as a temporary sink for trace metals in the environment and then release them when it dissolves (Welch et al., 2007).

The purpose of this study is to characterize a natural sample of jarosite from an acid sulfate soil site, and to experimentally determine the kinetics of acid and major ion release. Previous work on this material showed that trace elements were released to solution in dissolution experiments, however, there was a fractionation between trace metals compared to major ions (Welch et al., 2007). Ions that substitute into the A site (Rb^+, Sr^{2+} and La^{3+}) were preferentially released to solution in the initial stage of the dissolution reaction, whereas elements that substitute into the B site were preferentially retained in the solid phase.

Sediment cores rich in jarosite were collected from an acid sulfate soils site near Kempsey, on the mid north coast of New South Wales, Australia (30° 55′ 40″S, 152° 55′ 48″E). This area is within the lower Macleay River catchment where acid sulfate soils were first identified in Australia (Walker, 1972), and where highly vulnerable acid sulfate soils 'hotspots' have been targeted for management. Beavis et al. (2005) showed that acid discharge events from this site are highly responsive to rainfall. However, there can be a lag between the onset of rainfall and acidic discharge, as a function of antecedent moisture conditions—the drier the conditions, the longer the lag period. Once acidic discharge is initiated, poor water quality in terms of pH can persist for extended periods of time, from weeks to months. This relationship between rainfall and acidic discharge suggests that the kinetics of jarosite dissolution and the hydraulic conductivity of the sediments are major factors controlling acid discharge into the local waterways.

2. Methods

Jarosite dissolution experiments were conducted to estimate (a) kinetics of the reaction over a range of conditions relevant to acid sulfate soils and (b) the flux of acid and major ions to solution from jarosite.

2.1. Mineral identification

Jarosite was collected from sediment cores obtained from the field near Kempsey, New South Wales Australia. Intact sediment core samples were air-dried and then jarosite mottles were physically scraped from the bulk sediment. A jarosite powder sample was examined using a Cambridge S360 scanning electron microscope with EDXA capability, to determine bulk chemical composition and to visually estimate the purity of the jarosite powder. The powder sample was also analysed by XRD with a Siemens D500 series X-ray diffractometer, to confirm mineralogy. The remainder of the jarosite powder was gently disaggregated in a mortar and pestle to break up small clumps that formed as a result of air drying. Three subsamples of the powder, each ca. 2–10 mg in mass, were dissolved in 50% nitric acid to determine the bulk composition. These solutions were diluted in ~1% nitric acid and analysed for major and trace element composition by ICP-AES.

A separate core sample from the area was impregnated with resin, and cut into thick sections. The composition of the jarosite mottles was determined on approximately 25 spots by EDXA using a JEOL 6400 SEM. Because the sample was extremely porous and had previously been hydrous, totals were significantly less than 100%. Therefore, the data are presented as elemental ratios.

2.2. Dissolution experiments

For each of the jarosite dissolution experiments 200 mg of jarosite powder was placed in a clean polyethylene bottle, to which 100 ml of solution was added. There were six solution compositions used in the experimental treatments: (*i*) deionized water, (*ii*) 0.1 mM and (*iii*) 1 mM HCl (~pH 4 and 3), (*iv*) 0.05 mM and (*v*) 0.5 mM H_2SO_4 (~pH 4 and 3), and (*vi*) 1 mM oxalic acid (~pH 3). In the text, numbers *i*–*v* are referred to as 'inorganic' and *vi* is referred to as the 'organic' experiments. The oxalic acid was selected in order to determine the effects of organic acid on dissolution. These conditions were chosen in order to replicate the pH range that was encountered in the field site. Experiments were run in triplicate. After thorough mixing, the bottles were placed on an orbital shaker at ~100 rpm for the first 2 weeks of the experiment. 10 ml aliquots were removed periodically over 12 days to determine reaction kinetics, and a final sample was collected after 1 year. At each sampling interval, bottles were removed from the shaker approximately 1 h before sampling to allow the solid phase to settle. Samples were filtered, acidified with nitric acid to ~0.1% acid and analysed for major ions and total dissolved S (reported as SO_4^{2-}) by ICP-AES. Solution pH was measured on an aliquot of the filtered sample before acidification.

Residual solids at the end of the dissolution experiments (1 year samples) were analysed with either the Cambridge S360 SEM, or Hitachi 4300 SE/N (Schottky Field Emission SEM) to determine how the material had changed over time. A small aliquot of the powder slurry was placed on carbon tape and air-dried before analysis. Samples of the residual material were also dissolved in 50% nitric acid and analysed for major and trace element composition.

3. Results

3.1. Jarosite characterization

The jarosite powder extracted from the mottles was mustard yellow in colour. Analysis of this powder in the SEM showed that the sample appeared to be >95% jarosite that existed as individual euhedral crystals ranging in size from ~0.5 to 5 μm. There were minor amounts of clay (~ illite composition), gypsum, diatom fragments and quartz grains (Fig. 2) intermixed with the sample.

The chemical composition of the jarosite crystals as determined by EDXA spot analysis was consistent with the endmember composition, with peaks for K, Fe and S observed in similar proportions for all the analyses and no significant presence of Na was observed in the spectra. However, the analysis was only semi-quantitative due to the very small grain size and admixture with other phases, and it was not possible to determine the exact composition of the jarosite phase from these data. Minor Al peaks were observed to be strongly correlated with Si, and coincident with micron-sized platy minerals observed in the SEM images, indicating that the EDXA was detecting trace amounts of clays intermixed with the jarosite sample.

XRD analysis of the powder was consistent with the dominant phase being jarosite: the best fit to database patterns was for a hydronium substituted jarosite (K, H_3O^+)$Fe_3(SO_4)_2(OH)_6$ (Fig. 3). Quartz and illite were the other major phases identified by XRD, both of which were also observed by SEM. No other phases were apparent in the XRD spectra.

A subsample of the jarosite powder that was used for the dissolution experiments was completely digested in nitric acid. This aliquot appeared to have a composition different from that examined in the SEM (Table 1). This sample was relatively richer in sodium, with 1:1 average Na:K ratio. It was not possible to ascertain whether the Na and K were definitely present in the jarosite, precipitated salts, or another mineral phase that was intermixed with the jarosite. But given that other cations measured in this sample (such as Ca, Mg, Al, Si) were all <5% of the concentrations of {Na, K} which can occur as the major elements in jarosite, it was considered likely that the ~1:1 Na:K ratio reflected that of the jarosite starting material. The molal $(Na^+ + K^+)/SO_4^{2-}$ ratio in the digest was lower than the expected 1:2 ratio, indicating that either there was also hydronium (H_3O^+) substitution in the A site or there was another SO_4^{2-} phase present such as gypsum. The Fe^{3+}/SO_4^{2-} ratio was approximately 25% higher than expected for the stoichiometric jarosite composition, but this is reasonable for a natural sample in which the jarosite has undergone partial incongruent dissolution to form Fe oxyhydroxides. Neither goethite nor any other iron oxyhydroxide phase were observed in the XRD patterns, but a product of such a reaction would tend to be nanocrystalline, which gives rise to broad, diffuse XRD peaks that would not have been apparent above the background. The EDXA analysis in the SEM was not sufficiently quantitative to detect iron oxyhydroxide minerals intermixed with the jarosite powder.

The compositions of spot analyses of jarosite mottles from an intact core were extremely variable, ranging from Na- to K-endmember, with a mean Na:K composition of ~1.4:1 (Table 1). This is consistent with the observed pore water chemistry, where the measured Na:K ratios were on the order of 100:1 (Isaacson et al., 2006). The Fe^{3+}/SO_4^{2-} ratio was slightly lower than that of stoichiometric jarosite, indicating that either some of the Fe sites were substituted by other cations (Al) or were vacant, or that some of SO_4^{2-} was associated with other mineral phases. Fe substitution may be a factor: Al content of the jarosite could not be quantified due to the ubiquitous clay interspersed with the jarosite mottles. Other sulfate minerals are known to have been present. Gypsum is abundant at this site, and was observed with SEM analysis of the jarosite powder, indicating it could provide a repository for excess sulfate. In addition, other sulfate salts (Na, Mg, Fe or Al–SO_4^{2-}) are known to occur in acidic sulfate systems and have been observed at this site (e.g. Bigham and Nordstrom, 2000; and Welch, unpublished).

The difference in composition between the jarosite powder used for the dissolution experiments and the powder analysed in the SEM reflects spatial heterogeneity observed in the intact mottle sample. The powder used in the dissolution experiments reflects the average composition of a sample that was pooled from several different mottles within two separate cores taken within 10 m of each other.

Jarosite surface area was not determined experimentally on the starting material. SEM analysis of the starting material (Fig. 2) as well as analysis of other jarosite mottles from the field site (Welch unpublished) show that the jarosite mottles largely consisted of

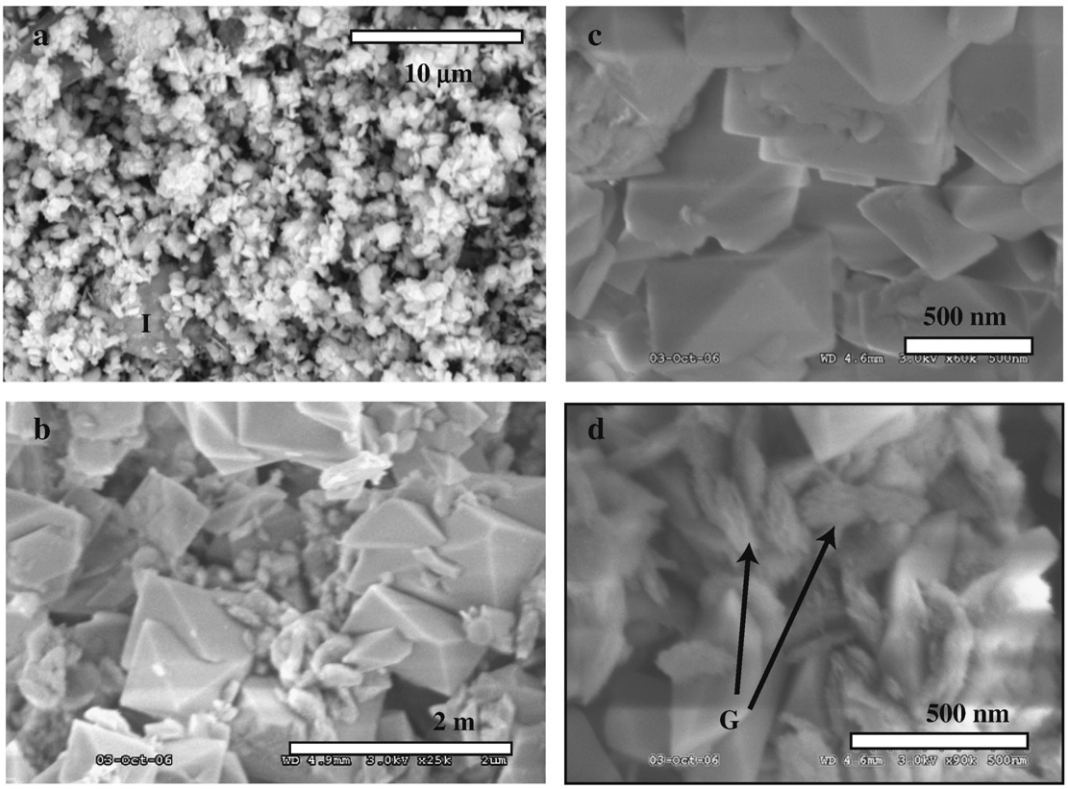

Fig. 2. SEM images of jarosite. The aggregation is the result of sample preparation, where a large amount of material was placed on a SEM stub. (a) Jarosite starting material showing some intermixed clay (I) with illite composition (b) higher magnification image of jarosite starting material showing euhedral crystals and distribution of grain size. (c) Jarosite reacted in pH 4 HCl experiment after 1 year, the smaller grain size particles that were observed in the starting material are less abundant in the reacted material. (d) Fe-rich precipitates in the reacted sample. The morphology of these precipitates is consistent with goethite, but the mineralogy was not confirmed.

relatively euhedral individual jarosite crystals ranging from approximately 0.5 to 5 µm size. If we assume that jarosite crystals approximate regular octahedra which have 1 µm centre-apex distance (Fig. 2), and that the density is close to the ideal 3.1 g/cm^3 (Barthelemy, 2000), then the geometric surface area is 1.68 m^2/g. This is closely comparable to the values of 1.3 m^2/g for the euhedral synthetics of Gasharova et al. (2005) and 1.4 m^2/g measured by the BET method for the spherulites of Smith et al. (2006c), but somewhat smaller than the 4 m^2/g of Sasaki and Konno (2000). The value of 2 m^2/g was used for estimating jarosite reaction rates normalized to initial mineral surface area in these experiments.

3.2. Experimental results of jarosite dissolution

Jarosite was reacted in deionized water, dilute hydrochloric acid and sulfuric acid at initial pH of ~3 and 4, and 1 mM oxalic acid (Fig. 4).

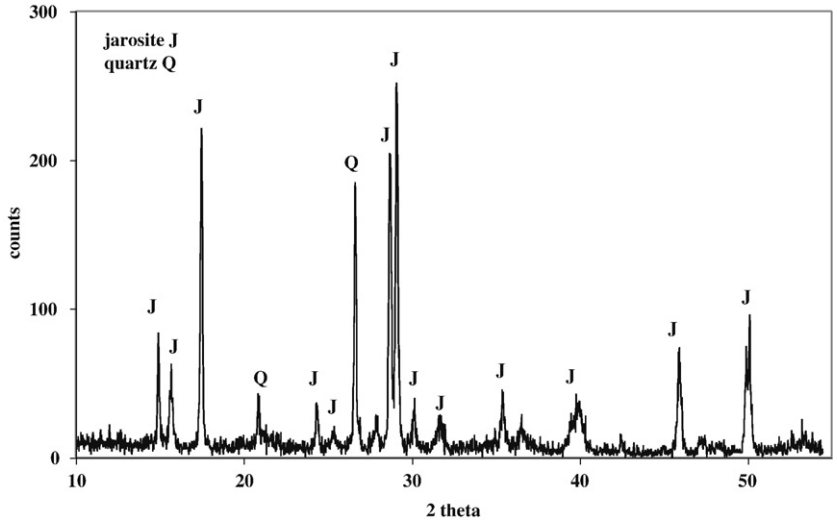

Fig. 3. XRD analysis of jarosite starting material (counts vs degrees 2θ). Peaks at ~21° and 27° correspond to quartz (Q); all other peaks above 20 counts correspond to a hydronium substituted jarosite (J).

Table 1
Mean composition of the initial and reacted jarosite determined by acid digestion, and mean composition of jarosite mottles determined in thin section from ca. 25 spot analyses

	$(Na+K)/SO_4^{2-}$	Fe/SO_4^{2-}	(Na+K)/Fe	Na/K
Initial	0.31	1.9	0.16	1.12
Reacted	0.31	1.9	0.16	1.09
Microprobe	0.44	1.4	0.31	1.43
Endmember	0.5	1.5	0.33	–

In all of the inorganic dissolution experiments, there was a rapid release of cations to solution within the first few hours followed by a much slower increase in concentration of major ions over the next 12 days. The initial rapid increase represents the dissolution of soluble salts that precipitated from the porewater as the sediment dried. The total dissolved salt concentrations released in the water, HCl at pH 3 and 4, and sulfuric acid pH 4 were similar after 12 days, in spite of the different initial conditions and different pH during the experiment. In contrast to these, in the oxalate experiment, the major solutes increased at a constant rate over the duration of the experiment, and total dissolved salt concentration was approximately an order of magnitude greater than the other experiments by the end of the 12 days.

The pH of the jarosite dissolution experiments changed over time (Fig. 4). In the water treatment, pH decreased from neutral to ca. 4.5 within minutes and then slowly decreased to pH 4 by the end of the experiment. In the experiments that started at pH 4, solution pH decreased slightly over the duration of the experiments, to pH 3.8–3.9 over 12 days. In the experiments starting at pH 3, pH increased immediately to ~3.1 and remained constant during the short-term experiments (0–12 days), to pH 3.1–3.2 (Table 2).

3.2.1. Reaction stoichiometry

The dissolution of jarosite was non-stoichiometric in all of the experiments, suggesting that there were other mineral phases intermixed with the jarosite, that the jarosite composition was variable, or that the reaction was incongruent, leading to the precipitation of secondary solids. Based on the SEM analysis of the solid phase, and the solution chemical analysis, it is likely that all

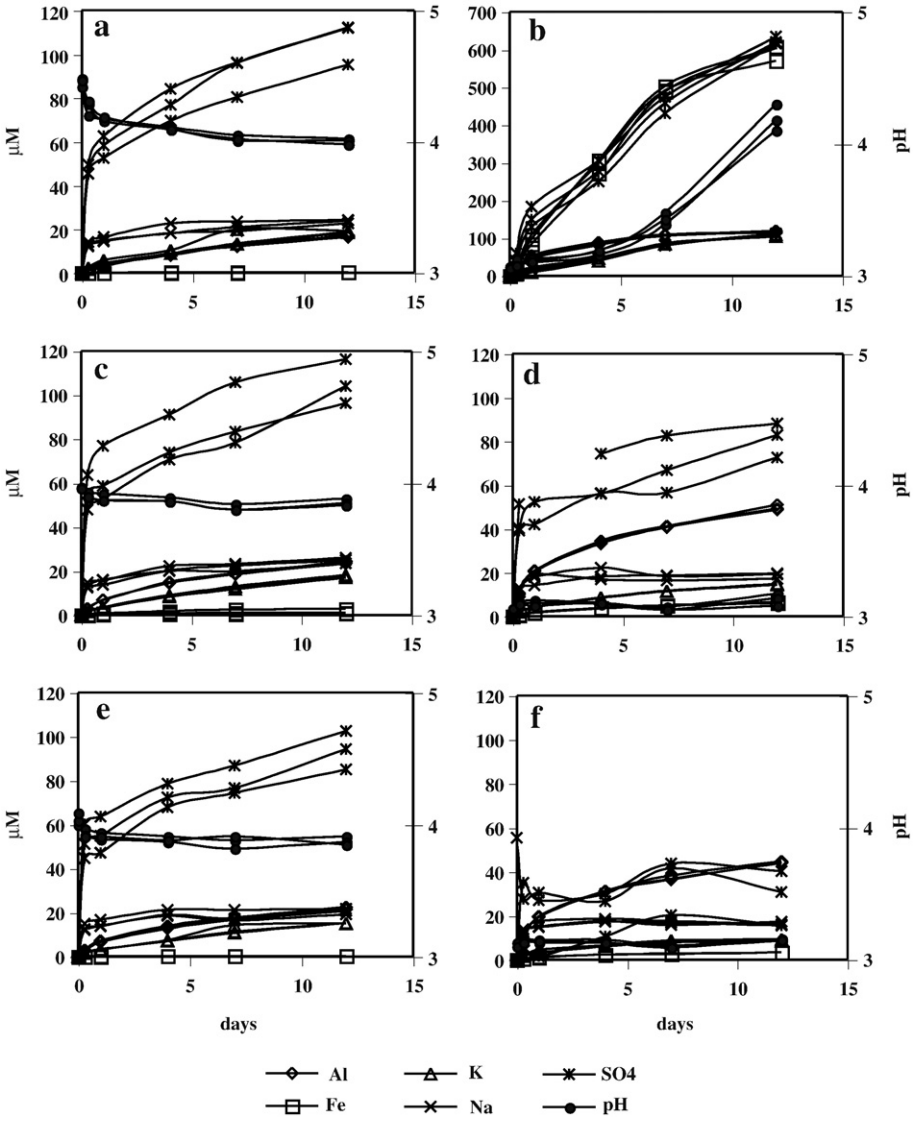

Fig. 4. Major ion concentration in the short-term jarosite dissolution experiments. The treatments were (a) water, (b) 1 mM oxalate, (c) HCl pH 4 (d) HCl pH 3 (e) H_2SO_4 pH 4 (f) H_2SO4 pH 3. Note that the data for the oxalate experiments are plotted on a different scale.

Table 2
(a) Mean concentrations of major ions and (b) major ion ratios at the end of 12 days ('12d') and 1 year ('final')

(a)	[Al]	[Fe]	[K]	[Na]	[SO_4]	[Si]	[Mg]	[Ca]	pH	[K+Na]
Water 12d	17.1	0.3	21.7	41.8	137	7.9	29.0	13.6	4.00	63.5
Water final	93	0.2	76.6	136	442	106	33.2	17.9	3.76	213
ox 12d	121	596	107	127	661	29.7	34.0	12.8	4.20	234
ox final	99	0.2	132	179	572	169	52.8	19.2	3.57	311
hcl 4 12d	24.4	1.5	18.1	39.2	125	8.0	28.8	13.6	3.85	57.4
hcl 4 final	100	0.3	73.9	125	423	106	31.6	17.1	3.63	199
hcl 3 12d	50.7	6.3	15.2	34.8	101	11.0	28.6	14.7	3.13	50.0
hcl 3 final	160	3.4	45.7	90.1	276	177	43.4	20.1	3.28	136
so4 4 12d	22.5	0.4	15.7	36.2	167	8.4	28.3	14.5	3.87	52.0
so4 4 final	99	0.3	71.2	120	465	112	31.6	18.3	3.62	191
so4 3 12d	45.1	3.4	9.3	32.6	528	11.5	28.7	15.1	3.15	41.9
so43 final	146.5	2.0	27.0	66.3	676	189	48.2	20.7	3.30	93.4

(b)	[K]/[K+Na]	[K+Na]/[SO_4]	[K]/[SO_4]	[Fe]/[Fe+Al]	[Fe+Al]/[SO_4]	[Fe]/[SO_4]	[Al]/[SO_4]	[Al]/[Si]
Water 12d	0.34	0.46	0.16	0.017	0.13	0.0022	0.13	2.16
Water final	0.36	0.48	0.17	0.002	0.21	0.0005	0.21	0.88
ox 12d	0.46	0.35	0.16	0.83	1.08	0.90	0.18	4.07
ox final	0.42	0.54	0.23	0.002	0.17	0.0004	0.17	0.59
hcl 4 12d	0.32	0.46	0.14	0.058	0.21	0.0120	0.20	3.05
hcl 4 final	0.37	0.47	0.17	0.003	0.24	0.0007	0.23	0.94
hcl 3 12d	0.30	0.50	0.15	0.110	0.56	0.0620	0.50	4.61
hcl 3 final	0.34	0.49	0.17	0.021	0.59	0.0124	0.59	0.90
so4 4 12d	0.30	0.31	0.09	0.017	0.14	0.0023	0.14	2.68
so4 4 final	0.37	0.41	0.15	0.003	0.21	0.0006	0.20	0.88
so4 3 12d	0.22	0.08	0.02	0.070	0.092	0.0064	0.09	3.92
so43 final	0.29	0.14	0.04	0.013	0.22	0.0029	0.22	0.78

All concentrations in μM.

three possibilities contributed to the non-stoichiometry of dissolution. The initial very rapid increase of Na^+, Mg^{2+}, Ca^{2+} and SO_4^{2-} is probably due to dissolution of soluble chloride and sulfate salts that had precipitated within the jarosite mottles when the core was dried. After this rapid increase, Mg^{2+} and Ca^{2+} concentrations were nearly constant over the next 11 days of the experiment. The majority of Na^+ concentration increase that occurred in the first 12 days occurred in the first day in the inorganic experiments. Based on results of the 1:5 sediment:water extracts from this site (Somerville et al., 2004), the Na^+, Ca^{2+} and Mg^{2+} contents of the solution due to soluble salts should be 0.5–1 ppm (~10–40 μM), which is about half the concentrations of these ions measured in the jarosite dissolution experiments. However from visual inspection of the core, the porosity of the jarosite mottles is greater than for the surrounding clay material, implying a greater proportion of saline pore water, which would give a correspondingly larger solute concentration. If the Ca^{2+} came from dissolution of gypsum, then approximately 10% of the total sulfate concentration in the water and HCl treatments could be from dissolving gypsum. We note that gypsum crystals were observed in the surrounding clay matrix, and a gypsum crystal was observed in the jarosite powder sample in the SEM.

Because of the occurrence of this salt dissolution pulse in the first day of the experiments, it was not always appropriate to measure reaction progress using the total cation and anion concentrations. Concentrations were corrected by subtracting the day 1 values when assessing the extent and stoichiometry of jarosite dissolution. However, the uncorrected total concentrations were retained for speciation calculations and are reported in tables.

Na^+ and H_3O^+ substitute for K^+, and Al^{3+} can substitute for Fe^{3+}, in the jarosite structure indicating that all of these cations may be released via dissolution. In the short-term experiments, Na^+ concentration increased only slightly after the initial salt pulse, although the Na^+ concentrations increased by approximately half that of K^+ from days 1 to 12 in the inorganic experiments (Fig. 4). The K^+/SO_4^{2-} ratio was lower than would be expected for stoichiometric endmember jarosite dissolution, approximately 1:3 rather than 1:2, indicating that approximately a third of the K^+ sites were replaced by Na^+ in the phase that was dissolving.

Although Al^{3+} can substitute for Fe^{3+} in the jarosite structure, another source of Al^{3+} in these experiments was from the dissolution of clay minerals that were intermixed with the jarosite mottles. Assuming that the clay has an Al:Si ratio near 1:1 as for kaolinite, $Al_2Si_2O_5(OH)_4$ and illite, ca. $(K,H_3O)_xAl_2[Al_xSi_{3+x}O_{10}](OH)_2$, the Si concentrations and Al/Si ratios imply that dissolution of clay minerals would account for approximately a third of the Al^{3+} released to solution in the first 12 days but the majority of Al^{3+} released more slowly over the full year (Table 2). The difference suggests that much of the early Al^{3+} in solution comes from fast-dissolving soluble Al minerals such as aluminocopiapite, alunogen or jurbanite that have been described in acid sulfate soils or in areas associate with acidification due to pyrite oxidation (Bigham and Nordstrom, 2000; Preda and Cox, 2004). The Al^{3+}/SO_4^{2-} ratio in the experiments other than sulfuric acid digests ranged from 0.13–0.59, higher than that of the jarosite, and in the HCl experiments, was higher at pH 3 than at pH 4, which could be the result of increased leaching of Al from clay phases.

The Fe^{3+} concentration in solution was about an order of magnitude higher at pH 3 than at pH 4, but was still much lower (<10%) than predicted for stoichiometric jarosite dissolution based on sulfate concentration. Even in the unlikely event that all of the Al^{3+} measured in the experiments was substituted into the Fe^{3+} site in jarosite, the $(Al^{3+}+Fe^{3+})/SO_4^{2-}$ ratio in solution would still be significantly less than the expected value 1.5 for stoichiometric dissolution (Table 2), which indicates that under the experimental conditions, jarosite dissolution is incongruent (Eq. (1)).

Thermodynamic calculations on the solution composition at the end of the kinetics experiments were carried out using the SpecE8 module of Geochemist's Workbench® (Bethke, 2006) and the Minteq database (Allison et al., 1991). The data base was modified to include log*K* values for aged ferrihydrite (Langmuir and Whittemore, 1971), schwertmannite (Majzlan et al., 2004) and an intermediate jarosite composition $(K_{0.67}Na_{0.33})Fe_3(SO_4)_2(OH)_6$ calculated from using ideal mixing on homologous sites from endmember composition.

Saturation indices were calculated as log(IAP/K_{eq}) (where IAP is the ion activity product) for dissolution reactions:

$$KFe_3(SO_4)_2(OH)_6(s) \rightarrow K^+(aq) + 3Fe^{3+}(aq) + 2SO_4^{2-}(aq) + 6OH^-(aq)$$

$$FeO(OH)(s) + H_2O \rightarrow Fe^{3+}(aq) + 3OH^-(aq)$$

and analogously the other jarosite and iron oxyhydroxide phases. Results of these calculations show that the solutions were greatly undersaturated with respect to potassium, hydronium and sodium jarosite endmembers, as well as an intermediate jarosite solid solution $(K_{0.67}Na_{0.33})Fe_3(SO_4)_2(OH)_6$, and were undersaturated to saturated with respect to amorphous $Fe(OH)_3$ but super-saturated with respect to goethite (Table 3). Although goethite should be the ultimate product of jarosite weathering, nanocrystalline Fe-oxyhydroxide phases such as ferrihydrite and schwertmannite form readily as metastable intermediates in acid sulfate soils environments (Acero et al., 2006). These phases are more soluble than goethite (Sullivan and Bush, 2004; Majzlan et al., 2004), and would be expected to control Fe^{3+} concentration over the short-term in the jarosite dissolution experiments.

3.2.2. Final experiment results

The solutions from all the experiments were sampled after 1 year to determine 'steady-state' conditions for jarosite solubility (Table 2). The solution pH was approximately 3.3 in the experiments that started at pH 3, and 3.6–3.7 for the water, oxalate, and initial pH 4 experiments. The concentrations of major ions associated with jarosite, Na^+, K^+, Al^{3+} and SO_4^{2-} were approximately 4–5 times higher after 1 year than the concentrations measured after 12 days in the inorganic experiments. However, it is clear that some of the increase in these ions, particularly Al^{3+}, could have come from dissolution of trace mineral phases intermixed within the jarosite. The Al:Si ratio was about 1:1 after a year, consistent with the slow dissolution of clay minerals in the acidic solutions. Potentially, some of the Na^+ and K^+ could also have come from dissolution of smectite clays, but the final $(Na^+ + K^+)/SO_4^{2-}$ for experiments without added sulfate was about 1:2, consistent with stoichiometric dissolution of jarosite {Na, K, S}. The Na:K ratio in the inorganic jarosite dissolution experiments after 1 year was variable: ca. 3:2 in the water and pH 4 experiments, and ca. 3:1 in the pH 3 experiments, which probably reflects slight compositional variation of jarosite powder. Na and K concentrations were lower at pH 3 than 4 (Table 2). Ca and Mg concentrations increased approximately 50% over the year, compared to the 5-fold increase in sulfate, suggesting that they were coming not from jarosite but from dissolution of other trace phases (such as gypsum in the case of Ca) or smectite.

In contrast to the other major elements in jarosite, dissolved Fe^{3+} concentrations decreased over time from their values at 12 days. Final concentrations were two orders of magnitude lower than stoichiometric relative to sulfate (Table 2): ~0.2 to 0.3 μM at pH 3.6 and ~2–3 μM at pH 3.3 after one year. The Fe^{3+} concentration in the oxalate experiment also decreased substantially over this time, from approximately 600 μM to 0.2 μM (Table 2) indicating the breakdown of Fe oxalate complexes over time. The decrease in Fe^{3+} concentration over the course of the experiments indicates precipitation of iron oxyhydroxide phases.

Table 3
Intermediate pH and saturation indices with respect to different mineral phases, calculated using the Minteq thermodynamic database for average solution composition after 12 days

Experiment	Final pH	$Fe(OH)_3$ amorph	Goethite	Alunite	Jar ss	Jar K	Jar Na	Jar H_3O
Water	4.00	−0.19	2.52	−2.43	−6.01	−4.50	−9.92	−9.44
HCl 4	3.85	0.30	3.01	−2.89	−4.27	−2.78	−8.15	−7.49
HCl 3	3.13	−0.33	2.38	−6.62	−4.38	−2.90	−8.24	−6.80
H_2SO_4 4	3.88	−0.25	2.46	−2.93	−5.77	−4.29	−9.63	−8.95
H_2SO_4 3	3.15	−0.67	2.03	−6.47	−4.16	−2.74	−7.89	−6.45

Table 4
Final pH and saturation indices with respect to different mineral phases, calculated using the Minteq thermodynamic database for average solution composition after 1 year

Experiment	Final pH	$Fe(OH)_3$ aged	Goethite	Alunite	Jar ss	Jar K	Jar Na	Jar H_3O
Water	3.76	−0.23	1.97	−0.96	−5.55	−4.03	−9.48	−9.26
HCl 4	3.63	−0.27	1.93	−1.66	−5.34	−3.82	−9.29	−8.91
HCl 3	3.28	0.17	2.37	−3.47	−3.69	−2.19	−7.59	−6.72
H_2SO_4 4	3.62	−0.29	1.91	−1.75	−5.31	−3.78	−9.26	−8.84
H_2SO_4 3	3.30	−0.10	2.10	−3.60	−3.87	−2.40	−7.71	−6.72

Solution speciation and saturation indices for experimental conditions after a year were calculated (Table 4) using SpecE8 with the Minteq database similar to the short experiments. Solutions were all supersaturated with respect to goethite but saturated with respect to aged ferrihydrite, indicating that goethite would ultimately be a stable product of incongruent dissolution of jarosite. Any metastable Fe oxyhydroxides present would tend to invert to goethite on standing, so goethite is the most likely final product of the reaction. The final concentrations show an inverse correlation between Fe^{3+} and SO_4^{2-}, indicating that solution composition may be limited by saturation with respect to some Fe^{3+} sulfate phase. This strongly suggests that schwertmannite, ca. $Fe_8^{3+}(SO_4)O_8(OH)_6$, or a similar compound precipitates as the initial metastable solid. All solutions are undersaturated with respect to the K^+, Na^+, H_3O^+ jarosite endmembers and intermediate jarosite composition, which implies that jarosite cannot be the buffering phase. The degree of undersaturation did not change markedly between day 12 and day 350, the increase in most major ions being compensated by the loss of Fe (Tables 2, 3, 4) and the change in acidity. Solution conditions approached saturation with respect to alunite due to the high Al concentration, particularly in the higher pH experiments: the saturation index ranged from −1 to −3.6. This indicates that the reaction path for jarosite dissolution in these long-term dissolution reactions may be controlled by precipitation of not only iron oxyhydroxides but also alunite, given the presence of clay impurities.

3.2.3. Kinetics of the dissolution reaction

3.2.3.1. Short-term jarosite dissolution rate. The kinetics of jarosite dissolution can be estimated from the change in solute concentration over time. For these estimates, it was assumed that the rapid increase in solutes in the first day of the experiments was largely due to dissolution of other salts that formed from the porewater as the core dried, and only the data from days 1–12 were used to calculate short-term jarosite dissolution rates. Mean jarosite dissolution rates were determined from a linear fit to both SO_4^{2-} and K^+ concentrations over time. Dissolved Fe and solution pH were not suitable indicators of degree of jarosite dissolution because Fe was known to precipitate slowly as an iron oxyhydroxide phases, which in turn affected solution acidity. Sodium was not used to calculate dissolution rates because of the relatively large background concentration from the dissolution of salts.

Jarosite dissolution rates based on sulfate release were very similar in all the inorganic experiments. Sulfate release rates ranged from 0.5 to 2.2 μmol SO_4^{2-}/g jarosite/day (Table 5, Fig. 4), which corresponds to a jarosite dissolution rate of 0.25–1.1 μmol jarosite/g jarosite/day. Reaction rates were slightly faster in water and dilute HCl (pH ~4), 0.95–1.1 μmol jarosite/g jarosite/day, than in HCl at pH ~3, where the rate was 0.65 μmol jarosite/g jarosite/day. Jarosite dissolution rates were slower in the presence of sulfuric acid than in the HCl treatment

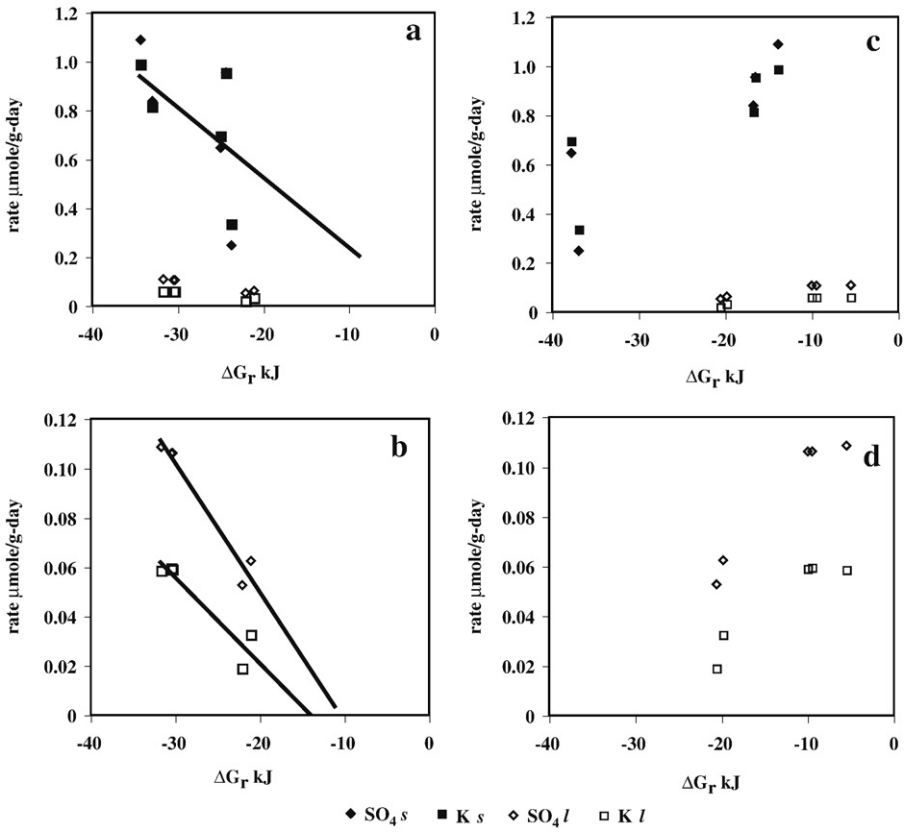

Fig. 5. Jarosite dissolution rate for the short-term (closed symbols ◆, ■) and long-term experiments (open symbols ○, □) versus ΔG_r calculated with respect to (a,b) an intermediate jarosite $(K_{0.67}Na_{0.33})Fe_3(SO_4)_2(OH)_6$ and (c,d) alunite $KAl_3(SO_4)_2(OH)_6$. ΔG_r was calculated from saturation index for solution composition conditions at T=12 days (short-term) and T=1 year (long-term) using SpecE8 module of Geochemist's Workbench® (Bethke, 2006) and the Minteq database (Allison et al., 1991). The data base was modified to include log$K$ values for aged ferrihydrite (Langmuir and Whittemore, 1971), schwertmannite (Majzlan et al., 2004) and an intermediate jarosite composition that matched the reaction stoichiometry of the short experiments. The stability constant for the intermediate jarosite solid solution (ss) was calculated from an ideal mixing model of the two endmembers.

at the same pH, 0.85 µmol/g jarosite/day at pH 4 and 0.25 at pH 3 versus 0.95 and 0.65 respectively, indicating that higher concentrations of sulfate inhibit the dissolution reaction, as would be expected since sulfate is a reaction product.

Similar results were obtained by determining rates based on K^+ concentrations in the inorganic experiments. K^+ release rates were approximately 1/3 the values for sulfate. Assuming that the reacting phase had a composition of $(K_{0.67}\ (Na,\ H_3O^+)_{0.33})Fe_3(SO_4)_2(OH)_6$, the molar K:S ratio in jarosite was 1:3, so jarosite reaction rates for all the inorganic experiments were similar for dissolution rates whether calculated from either SO_4^{2-} or K^+ concentration in solution (Fig. 5, Table 5). The fastest reaction rates were associated with greatest degree of undersaturation. Free energy of the dissolution reaction, ΔG_r, was calculated from the saturation index (SI), log(IAP/K_{eq}), with respect to the K, Na, and H_3O endmember jarosite compositions as well as an intermediate solid solution composition ($K_{0.67}Na_{0.33}$):

$$\Delta G_r = RT\ln(\mathrm{IAP}/K_{eq}) = 2.303RT \times \mathrm{SI} \quad (3)$$

Because of the possible simultaneous operation of congruent and incongruent dissolution mechanisms, no attempt was made to fit jarosite dissolution to a simple power-law rate equation. Mean rates were calculated from the change in solution composition from day 1 to day 12 of the experiments. This was found to be a reasonable empirical methodology, since release rates of SO_4^{2-} and K^+ did in fact appear to be relatively constant over the duration of the experiment. Linear extrapolation of jarosite dissolution rate versus ΔG_r based on the intermediate jarosite composition approached zero at ΔG_r=0 (Fig. 5). Equilibrium was evidently not obtained after 12 days: jarosite continued to dissolve over the rest of the year, albeit at a slower rate.

The effect of the individual product species measured at the end of the short experiments (day 12) versus jarosite reaction rates over day 1–day 12 are depicted in Fig. 6. There is a good linear correlation between reaction rate and pH at the end of the short experiments, reaction rates decreasing with increasing acidity. Similarly, reaction rates decrease with increasing concentration of the product species SO_4^{2-} and Fe^{3+}, even when total Fe^{3+} concentrations are approximately two orders of magnitude lower than SO_4^{2-}. Jarosite reaction rates appear to be insensitive to K^+ in solution. The fastest dissolution rates are associated with the highest final K^+ concentrations, but this is because they are associated with the greatest degree of dissolution, and K^+ is largely derived from the dissolution reaction. In the short-

Table 5
Estimates of jarosite dissolution rates from a linear regression of K^+ and SO_4^{2-} concentrations in solution in the short-term experiments in µmol/g jarosite/day

	Rate based on SO_4^{2-}	Rate based on K^+
Water	1.09±0.10	0.99±0.21
Oxalate	10.9±0.4	6.53±0.54
HCl pH 4	0.95±0.11	0.95±0.04
HCl pH 3	0.65±0.11	0.69±0.04
SO_4 pH 4	0.84±0.11	0.81±0.07
SO_4 pH 3	0.25±0.23	0.33±0.05

Rates are normalized per mole of jarosite assuming a jarosite composition of $(K_{0.67}\ (Na,\ H_3O^+)^{0.33})Fe_3(SO_4)_2(OH)_6$.

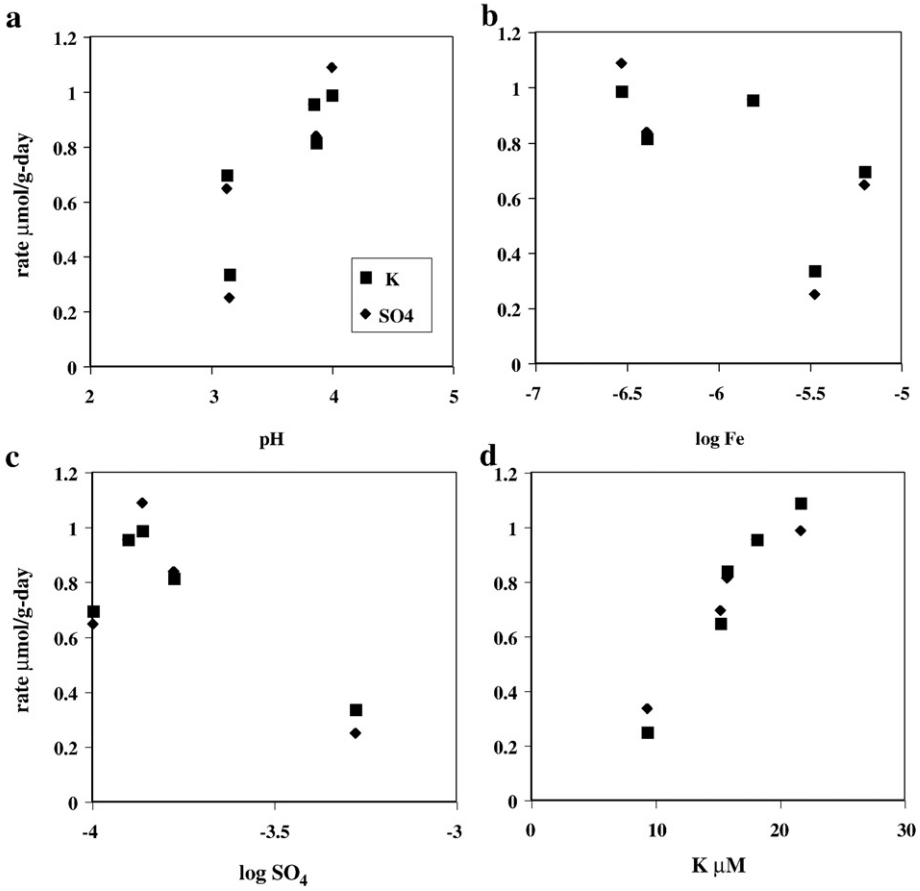

Fig. 6. Jarosite dissolution rates in the short-term experiments versus (a) pH, (b) log Fe^{3+} (µM), (c) log SO_4^{2-} (µM) and (d) K^+ (µM) concentrations at the end of the short-term experiments.

term experiments, increasing sulfate from 0 to 50 µM at pH ~4 had a minimal affect on reaction rate, whereas the larger increase from 0 to 500 µM SO_4^{2-} at pH 3 inhibited rate by a factor of about 2, although this pattern is complicated by the effects of Fe concentration and pH (Figs. 4, 6).

3.2.3.2. Long-term jarosite dissolution rate. The long-term jarosite dissolution rate was estimated from the change in concentration of K^+ and SO_4^{2-} from 12 to 350 days. Jarosite dissolution rates were approximately an order of magnitude slower than the rates determined in the short-term experiments, but the overall trends were similar to those observed for the preliminary phase of the experiments (Table 5, Fig. 5c). Sulfate release rates ranged from 0. 05–0.11 µmol/g jarosite/day. Rates were faster at higher pH than lower pH: 0.1–0.11 µmol/g jarosite/day compared to 0.05 to 0.06 µmol/g jarosite/day. In contrast to the short-term experiments, sulfate concentration had little inhibitory affect on jarosite dissolution rates, reaction rates were similar with or without added SO_4^{2-}. Similar trends were observed for K^+ release rates over duration of the experiment.

The stoichiometry of the reaction was markedly different in the long-term segment of the experiments compared to the short-term reaction. The K^+ release rate was only 20% that for sulfate, substantially lower than the 50% that would be expected from the stoichiometric dissolution of endmember jarosite, or the 33% that would have been expected based on the stoichiometry of the short-term dissolution experiments. The solution composition of the long-term experiments was more similar to the bulk composition of the starting material than that observed for the short experiments.

The free energy of the reaction ΔG_r at day 350 of the long-term experiments was calculated from the saturation index with respect to the endmember and intermediate jarosite composition, as well as for alunite. The ΔG_r values calculated for the long-term experiments differed little from those calculated for the short-term experiments (Tables 3, 4 and Fig. 5). Overall trends were found to be similar: there is a general decrease in reaction rate correlated with increasingly positive ΔG_r, and release rates for both K^+ and SO_4^{2-} approach 0 as ΔG_r with respect to the intermediate jarosite composition tends toward 0.

In contrast to the plots of rate versus jarosite saturation, plots of rate versus ΔG_r for alunite dissolution showed an increase in rate as solutions approached alunite saturation (Fig. 5). This apparently counterintuitive result arises since no alunite was physically present, the degree of alunite saturation was determined primarily by SO_4^{2-} release from jarosite and Al^{3+} release from clay, and hence saturation was most closely approached in the late, slow stages of jarosite dissolution. Jarosite dissolution was not significantly affected by the amount of Al^{3+} present.

3.2.3.3. Jarosite dissolution in oxalate. Jarosite dissolution kinetics in the oxalic acid solution was an order of magnitude faster than in the inorganic short-term experiments. Oxalate complexes readily with cations in the mineral surface and in solution, thus increasing dissolution rate and extent by both catalysis and by changing the solution saturation state. Oxalate markedly increases Fe^{3+} and Al^{3+} release to solution (cf. Welch and Ullman, 1993). Based on the change in solution stoichiometry in the oxalate experiments compared to the inorganic experiments, the major affect of oxalate is to solubilize Fe^{3+}. The oxalate experiment after 12 days is the only one in which Fe/S>0.1 (Table 2).

4. Discussion

The experimental data show that the stoichiometry and kinetics of jarosite dissolution are complex functions of solution composition. There are important implications for managing sites that contain jarosite, since jarosite reacts with water to release acid, salts, and trace metals. The rate of release of these components depends on the environmental conditions of the site, as well as on the composition of the jarosite.

4.1. Stoichiometry

4.1.1. Jarosite composition

The non-stoichiometric nature of jarosite has been noted in both laboratory and field conditions (Baron and Palmer, 1996; Smith et al., 2006a, c; Papike et al., 2006a, b). Jarosite rarely has ideal endmember stoichiometry: hydronium ion (H_3O^+) and Na^+ readily substitute into the K^+ site, giving a mineral composition that has K^+:SO_4^{2-} ratio <1:2. Similarly, substitutions at the Fe^{3+} site are also common in natural samples. These may be isovalent (e.g. Al^{3+}), but divalent cations (e.g. Cu^{2+}) can also be accommodated if charge balance is maintained by substitution of alkaline earths/lanthanides for K^+ or further protonation of hydroxyl groups. As many as 14% of the B sites can be vacant; these also are presumably charge-balanced by protons (Drouet and Navrotsky, 2003; Drouet et al., 2004; Basciano and Peterson, 2007). Hence, there is a high degree of variability in the composition of jarosite minerals, which will in turn have an effect on aqueous K:Fe:S ratios during dissolution.

4.1.2. Fe solution stoichiometry

The stoichiometry of the jarosite dissolution reaction in these experiments varies as a function of pH and also as a function of time. The pH-dependence of the reaction stoichiometry is largely related to the speciation of dissolved Fe^{3+} and the solubility of any secondary Fe–(O,OH) mineral phase. Jarosite dissolution can be described by a number of different reactions, depending on solution pH. The importance of pH is illustrated in the three reaction mechanisms implied by the experimental data.

At relatively high pH conditions (pH >4), jarosite dissolves incongruently to produce acidity:

$$KFe_3(SO_4)_2(OH)_6 + 3H_2O \rightarrow 3Fe(OH)_3\downarrow + 2SO_4^{2-} + 3H^+ + K^+ \quad (4)$$

Under extremely acidic conditions, jarosite is more likely to dissolve congruently to consume acidity and produce soluble ferric iron.

$$KFe_3(SO_4)_2(OH)_6 + 6H^+ \rightarrow 3Fe^{3+} + 2SO_4^{2-} + K^+ + 6H_2O \quad (5)$$

Some shift towards the latter behaviour is evident in the early phase of the experiments started at pH 3, where pH increased and dissolved Fe was detected in solution. This reaction has important implications for mobilizing acidity 'offsite', because the subsequent precipitation of Fe(OH) phases will generate acid:

$$Fe^{3+} + 3H_2O \rightarrow Fe(OH)_3 + 3H^+ \quad (6)$$

At pH >~3.7 $Fe(OH)_2{\cdot}4(H_2O)^+$ is the dominant species, and total Fe concentration is below saturation with respect to iron oxyhydroxide phase, the jarosite reaction can proceed without changing pH.

$$KFe_3(SO_4)_2(OH)_6 + 4H_2O \rightarrow 3Fe(OH)_2{\cdot}4(H_2O)^+ + 2SO_4^{2-} + K^+ \quad (7)$$

Fig. 7a,b shows the solutions at 12 days and after 1 year plot at or near equilibrium with ferrihydrite and aged ferrihydrite respectively. A detailed plot of the solution composition for the water experiment from 0.3 to 12 days shows that the progression is controlled by ferrihydrite precipitation clearly indicating that the incongruent reaction dominates the Fe concentration and pH (Fig. 7b). Schwertmannite is supersaturated and the data all situate within the schwertmannite stability field suggesting either a kinetic control or surface diffusion control giving preference to ferrihydrite precipitation (Fig. 7d). At 1 year the system is influenced by aged ferrihydrite, the ripening product of ferrihydrite (Langmuir and Whittemore, 1971). Schwertmannite saturation is achieved for the higher pH experiments at 1 year but the similarity in rate data based on K^+ and SO_4^{2-} release suggest schwertmannite precipitation does not play a significant role in controlling the solution composition. The data of Baron and Palmer (1996) suggests that schwertmannite precipitation occurred in their higher pH experiment with synthetic jarosite. This may be the result of the smaller crystal size of synthetic jarosite versus natural jarosite and thus reflect a kinetic control on which product phase forms. In our experiments, initially congruent dissolution results in precipitation of iron oxyhydroxide in minutes to hours, and dissolution of jarosite continues incongruently, producing acid. The data from prior to day 12 are undersaturated with respect to ferrihydrite but Fe content is several orders of magnitude below that for stoichiometric dissolution of jarosite. The low Fe content and the fact that the solution is undersaturated indicate that a jarosite mineral surface precipitation phenomena control the release of Fe to solution. At 12 days the solution is in equilibrium with ferrihydrite and disequilibrium between the solution and the mineral surface reactions no longer exists.

Although K^+, Na^+ and SO_4^{2-} concentrations increased substantially over the year, the total Fe concentration decreased. This implies that the stoichiometry of the reaction evolved from an initial, very short-lived congruent stage to continuously increasing degrees of incongruence due to slow precipitation of a secondary iron mineral phase. Metastable iron mineral phases such as ferrihydrite or schwertmannite are likely to form first, and then age to more stable (less soluble) forms ultimately leading to goethite (cf. Banfield et al., 2000; Acero et al., 2006). This is consistent with observations of acid sulfate soils systems, where schwertmannite and 'amorphous iron oxyhydroxide phases' form rapidly by oxidation of pyrite and FeS but then slowly age to goethite (Sullivan and Bush, 2004). The differing solubilities of the Fe oxyhydroxides can be seen in Fig. 7c. The complex path towards jarosite saturation is summarised in Fig. 8, which includes analytical data for the first few hours and days of jarosite dissolution in water. Several phases of dissolution can be distinguished:

(*i*) [SO_4^{2-}] was already high within the first few hours, due to dissolution of soluble salt impurities.
(*ii*) During the first few days, [Fe^{3+}] and [SO_4^{2-}] increase, due to dissolution of jarosite but Fe release is slow as ferrihydrite precipitates. The saturation index of jarosite increased relatively rapidly.
(*iii*) At 12 days, the solution is in equilibrium with ferrihydrite as the predominant reaction is incongruent jarosite dissolution and [SO_4^{2-}] continued to rise. There was little change in saturation index of jarosite in this phase, which continued through the rest of the year.
(*iv*) After 1 year, aged ferrihydrite equilibrium controls the solution Fe composition (see Figs. 7c and 8). Extrapolation of the path suggests that after several years, jarosite saturation would be reached.

Note that the maximum transient Fe^{3+} concentration attained was therefore higher than if jarosite had decomposed immediately into a solid Fe crystalline oxyhydroxide. This distinction is important for managing acidic sites that have abundant jarosite, because jarosite dissolution can evidently produce substantial aqueous Fe^{3+}, which can catalyse pyrite oxidation. Flooding acid sulfate soils with the intent to limit further pyrite oxidation may therefore actually catalyse the pyrite oxidation reaction. Precipitates with morphology characteristic of goethite were observed in reacted jarosite samples in the SEM,

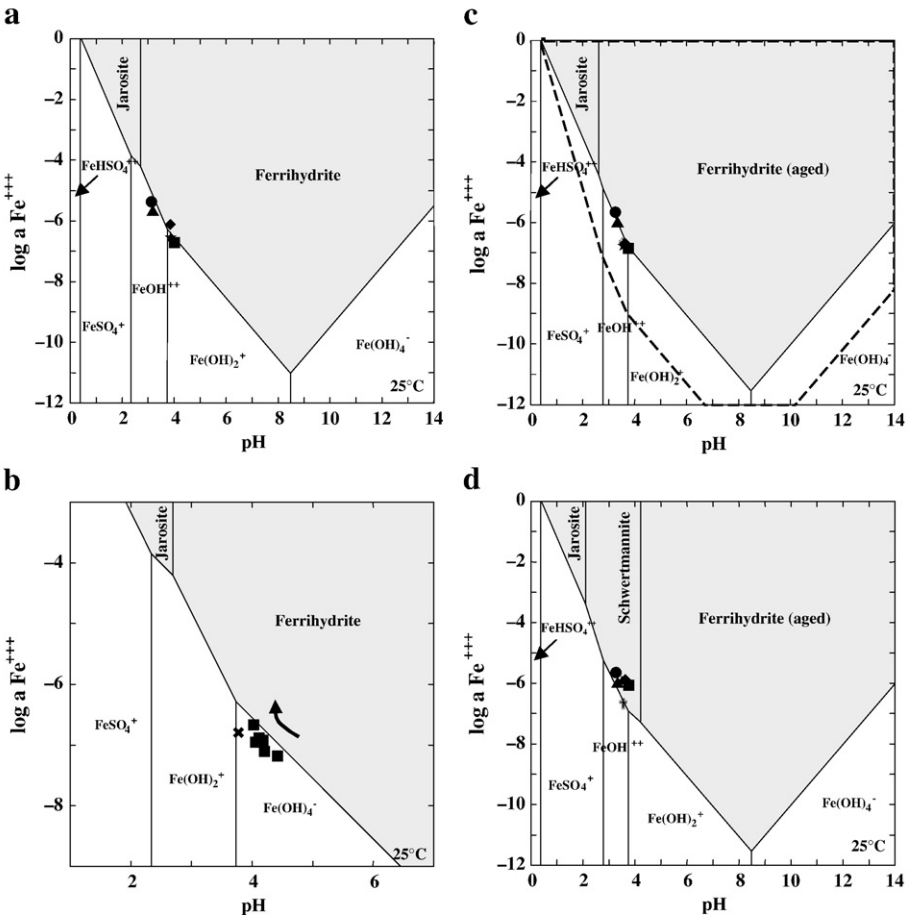

Fig. 7. a) Plot of pH vs activity of Fe species showing the stability fields for jarosite and ferrihydrite with the data for the water (■), HCl (4 ◆, 3 ●) and H_2SO_4 (4 ★, 3 ▲) experiments at 12 days superimposed. The data plot on or very near to the equilibrium curve for ferrihydrite. b) Similar to a) but showing the data for 0.3, 1, 4, 7 and 12 days (■) and 1 year (✖) for the water experiment. The data all plot below the ferrihydrite curve except for the day 12 data. c) Same as a) but with the stability field of aged ferrihydrite plotted and the goethite field superimposed (dashed line) and the 1 year data for the water, HCl and H_2SO_4 experiments. This data plots on or near the aged ferrihydrite equilibrium curve. d) Same as c) but with the stability field of schwertmannite included. The data plot predominantly within the schwertmannite field.

implying that discrete dissolution and reprecipitation reactions occurred. However, these oxyhydroxide precipitates were not abundant. We deduce that the majority of iron-rich residuum was intimately intergrown with and not readily distinguishable from the parent jarosite. This can occur if the intergrowth is on the submicron scale, and/or if the initial (metastable) residuum is jarosite-like in structure. Smith et al. (2006c) described the preferential leaching of K^+ and SO_4^{2-} from jarosite in batch dissolution experiments at pH 8, leaving behind the octahedral Fe-oxyhydroxide sheet. However this conclusion was based on solution composition, not on the observation of the product phase. SEM analysis on their reacted material showed rod shaped secondary precipitates on the mineral surfaces that had characteristic goethite morphology, similar to the ones observed here (Fig. 2).

4.1.3. Stoichiometry of dissolution

The stoichiometry of the cation release apparently changed between the short-term and the long-term dissolution of jarosite in the batch reactors. Over days 1–12 of dissolution for the inorganic experiments, the corrected cation concentrations in solution gave a Na:K:S ratio of approximately 0.3:0.7:2. However, the solution composition in the long-term jarosite dissolution experiment after 350 days had a Na:K ratio that was closer to 50:50. The increase in K/Na in the short experiments is surprising, since if both cations are of comparable concentration, and are released from the same solid by the same mechanism, one would expect faster release of the cation corresponding to the more soluble endmember. Both hydronium and sodium jarosite endmembers are much more soluble than potassium jarosite (log*K* values for dissolution from the Minteq database for

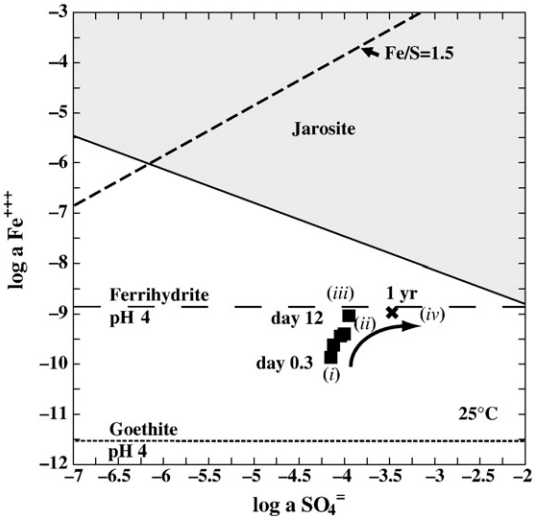

Fig. 8. Plot of $[Fe^{3+}]$ versus $[SO_4^{2-}]$, showing complex reaction path for dissolution of jarosite in water. Regions *i* through *iv* are described in the text. Symbols are for the data for 0.3, 1, 4, 7 and 12 days (■) and 1 year (✖) for the water experiment.

these minerals are −11.0 for jarosite, −5.30 for Na-jarosite, −5.39 for H_3O-jarosite, and −1.4 for alunite; Allison et al., 1991). Jarosite dissolution experiments by Gasharova et al. (2005) showed a factor 3 faster release of H_3O^+ from hydronium-jarosite relative to K^+ from jarosite into distilled water under similar conditions, which is consistent with the correlation for solubility.

There are several possible reasons for the change in Na:K ratio through time. The most likely possibility is a corresponding change in the composition of the jarosite that was dissolving. A shift towards more K-rich compositions would occur if jarosite grains were zoned with cores that were richer in K, or if K-rich grains were larger and tended to dissolve more slowly. As discussed above, the jarosite is known to have been heterogeneous in composition and crystal size, and SEM analysis of the reacted jarosite show that the smaller particle size fraction that was observed in the starting material was less abundant in the reacted material (Fig. 2).

Alternatively, some of the Na and K could have come from other mineral phases such as clays. Smectite and illite clays can behave as sources or sinks for alkali cations in solution by ion exchange. Substantial Si and Al increase over the year-long experiment indicated dissolution of aluminosilicate minerals (Table 2). If the clay was all of illite composition, about half of the K^+ in solution after 1 year could have come from the dissolution of clays.

4.2. Kinetics

The results of the jarosite dissolution experiments show that the kinetics of jarosite dissolution and acid production is a complex function of solution composition. While there have been several studies that have focused on the stability of jarosite, and have determined thermodynamic properties of natural and synthetic jarosite or jarosite group minerals (Baron and Palmer, 1996; Drouet and Navrotsky, 2003; Gaboreau and Viellard, 2004), few studies have focused specifically on the kinetics of jarosite reactivity.

4.2.1. Comparisons with other studies

The results of the inorganic jarosite dissolution experiments are broadly similar to other experimental studies that have been run under a range of conditions. For example, Smith et al. (2006c) describe the dissolution of synthetic jarosite at pH 2 and 8 in batch experiments. They found that the initial fast release of K^+ and SO_4^{2-} to solution decreased smoothly, and solution composition reaches a 'steady-state' after approximately 3000 h. If $\log[SO_4^{2-}]$ is used as a proxy for reaction progress and ΔG_r, their reaction rates are found to vary as a linear function of this parameter, as reported above for the data of this study. The dissolution rate of jarosite when SO_4^{2-} concentration was a factor of 10 below saturation can be estimated as 21 μmol/g/day for the pH 2 and 11 μmol/g/day for the pH 8 experiments. Given their surface area of 1.4 m^2/g, and assuming a jarosite density of 3.1 g/cm^3 and molar mass of 500 g/mol, these rates equate to mean surface recession velocities of $28–15\times10^{-15}$ m/s respectively.

These rates are about an order of magnitude faster than the rates determined for this study, which ranged from 0.5–2 μmol/g/day, even though our surface area is likely to have been similar to that in Smith et al. (2006c). This disparity is attributed to the differences in the starting material and differences in solution composition. The material used in the Smith et al. (2006c) study was a fresh, spherulitic synthetic jarosite. The spherules were similar in diameter to our crystals, but their constituent crystallites were much smaller, with greater surface roughness (cf. Fig. 3 in Smith et al., 2006c) than the natural material used in this study. The experiments by Smith et al. (2006c) were also run at pH conditions 2 and 8, above and below those used in this study at pH 3 and 4. This could be a contributing factor to the difference in reaction rates determined in the two studies since most minerals exhibit a pH-dependence on reaction rate (see below). It is further possible that our natural jarosite also had an inhibitory surface coating that reduced its effective surface area.

Gasharova et al. (2005) determined the dissolution rate of euhedral synthetic jarosite in an *in situ* AFM study. The calculated dissolution rates based on the retreat of {012} crystal faces in water were 4.4×10^{-7} and 1.45×10^{-7} mol/m^2 s for faces of H_3O^+ and K^+ dominant jarosite respectively, which correspond to effective surface recession velocities of 7.1×10^{-11} and 2.3×10^{-11} m/s. If the surface area of the jarosite used in our study is taken to be 2 m^2/g, then the recession velocities were $0.5–2\times10^{-15}$ m/s, which is 4–5 orders of magnitude slower than the rates of Gasharova et al. (2005). Gasharova et al. (2005) also calculate a bulk jarosite dissolution rate at pH 2 from the experiments of Baron and Palmer (1996) of 3×10^{-9} mol/m^2 s. This is still approximately 2 orders of magnitude faster than the rates determined in our experiments, but comparable to the rates we calculate from the experimental data of Smith et al. (2006c). It is evident that the jarosite of the present study dissolved very slowly relative to freshly prepared synthetic material, whether the latter was euhedral or spherulitic in habit. The differences in reactivity between synthetic or fresh mineral surfaces and naturally weathered samples have been well documented for silicate minerals (cf Casey et al., 1993; Velbel, 1993; White and Brantley, 2003).

4.2.2. Factors affecting jarosite reactivity

The speciation of Fe in solution, the stability of Fe mineral phases, and the formation of passivating Fe mineral films on the reacting mineral surface are major factors affecting jarosite reaction rates. The activities of non-Fe components in solution can also have a major effect on the thermodynamics and kinetics. For instance, experiments show that for many minerals, dissolution rates track solubility, and are a complex function of solution pH. The dissolution rates of most iron or aluminosilicate minerals are lowest at near-neutral pH ~5 to 8, and then increase with either increasing acidity or increasing alkalinity. The centre of this U-shaped curve reflects the pH of zero charge of the mineral surface, and the minimum in solubility of Fe(OOH) and aluminous mineral phases at near-neutral pH. However, jarosite reactivity as a function of pH is more complicated because of the overlapping mineral stability fields for jarosite, goethite, schwertmannite and ferrihydrite (Fig. 7). There is a change in the reaction mechanism at pH ~3.7 from incongruent dissolution precipitating a Fe–(O,OH) solid (Eq. (4)) to congruent dissolution (Eq. (5)).

Based on the mineral stability diagram we would expect to see jarosite reaction rates increase significantly below pH 2 where Fe^{3+} is the dominant ion in solution, and the slope of the jarosite stability limit on the $\log a_{Fe}$ vs pH plot changes. Jarosite dissolution rate estimates from Smith et al. (2006c) and Baron and Palmer (1996) at pH 2 are 1–2 orders of magnitude faster than the rates determined in our experiments, consistent with this prediction. However, the rates of Smith et al. (2006c) were also comparably fast at pH 8, suggesting that another factor is responsible for the difference in reactivity between their jarosite and ours, at least in the basic solutions.

The long-term and short-term dissolution experiments show that the jarosite reaction rate slowed down through time. Empirically, it was an approximately logarithmic function of the undersaturation. However, the path towards equilibrium was highly nonlinear. Analyses show that first, sulfate rose due to dissolution of soluble salt impurities within hours. Then, near-congruent dissolution of jarosite released Fe^{3+} and SO_4^{2-} into solution during the first few days. Then, dissolution became incongruent, and Fe^{3+} decreased while SO_4^{2-} increased, with little overall change in saturation index between 2 weeks and 1 year (Fig. 8). However, there were major changes in solution and solid composition over this time. Acidity was either generated (pH 4) or consumed (pH 3) as the reaction continued. The change in stoichiometry over time indicates that an iron-rich residuum forms; the slow reaction rate is likely due to some of this forming a passivating layer on the mineral surface.

This has implications for jarosite reactivity under natural conditions, and may explain the difference in reactivity between the natural jarosite used in this study and the much faster reaction rates determined for clean-surfaced synthetic jarosite used in other studies. Our natural jarosite would have had Fe–(OOH) phases associated with it, which would have reduced the reaction rate. Similar inhibitory phenomena have been observed for Fe^{3+} on fayalite (Santelli et al., 2001; Wogelius and Walther, 1992) and Al^{3+} on feldspar (Oelkers et al., 1994).

5. Summary and conclusions

The dissolution rate of a natural jarosite sample was determined in inorganic acids at pH 3 and 4, and in oxalic acid. Dissolution rates ranged from 0.25 to 1.1 μmol/g/day in the inorganic experiments, and rates were approximately an order of magnitude greater in the oxalate experiment. The dissolution reaction was non-stoichiometric over the course of the experiment: cations in the A site (H_3O^+, Na^+ and K^+) and SO_4^{2-} are preferentially leached from the mineral surface, leaving behind a residual Fe–(OOH) phase which may have been similar to ferrihydrite. Replacement and coating of jarosite by such material is likely the reason for the low reaction rate relative to the clean jarosites of other studies.

The results of these experiments have implications for managing natural environments that contain jarosite, such as acid mine drainage or acid sulfate soils. The experimentally determined dissolution rates on fresh synthetic samples are at least an order of magnitude faster than the rates determined for natural 'weathered' samples. Similar differences have been shown for fresh versus weathered silicate minerals (e.g. Casey et al., 1993; Velbel, 1993). Hence, jarosite will persist in natural environments for longer than would be predicted from laboratory dissolution experiments. However, the shift in dissolution mechanism after a few days from near-congruent to incongruent means that some mobile Fe^{3+} is generated which can spread acidity away from the dissolving jarosite. This could be very important for managing sites that have both pyrite and jarosite because Fe^{3+} can oxidize pyrite in the absence of oxygen, and can result in further acidification of affected sites.

Acknowledgements

Funding was provided by the Cooperative Research Centre for Landscape Environments and Mineral Exploration (CRC LEME). We would like to thank Ulli Troitzsch and Linda McMorrow for help with analysis with sediments and solutions respectively. SEM analysis was done at the Electron Microscopy Unit at the Research School of Biological Sciences ANU. We would like to thank Sally Stowe, Frank Brink and Cheng Huang for their assistance. We would like to thank Russel and Georgina Yerbury for their continued patience and for allowing us access to their property. Comments from associate editor Jeremy Fein, as well as from two anonymous reviewers, improved the manuscript.

References

Acero, P., Ayora, C., Torrento, C., Nieto, J.-M., 2006. The behavior of trace elements during schwertmannite precipitation and subsequent transformation into goethite and jarosite. Geochim. Cosmochim. Acta 70, 4130–4139.

Allison, J.D., Brown, D.S., Novo-Gradac, K.J., 1991. MINTEQA2/PRODEFA2, a geochemical assessment model for environmental systems: version 3.0 user's manual. U.S. Environmental Protection Agency Report EPA/600/3-91/021. 107 pp.

Alpers, C.N., Rye, R.O., Nordstrom, D.K., White, L.D., King, B., 1992. Chemical, crystallographic and stable isotopic properties of alunite and jarosite from acid-hypersaline Australian lakes. Chem. Geol. 96, 203–226.

Banfield, J.F., Welch, S.A., Zhang, H., Thomsen Ebert, T., Penn, R.L., 2000. Aggregation-based crystal growth and microstructure development in natural iron oxyhydroxide biomineralization products. Science 289, 751–754.

Baron, D., Palmer, C.D., 1996. Solubility of jarosite at 4–35 °C. Geochim. Cosmochim. Acta 60, 185–195.

Barthelemy, D., 2000. Webmineral database. http://www.webmineral.com, cited in May 2007.

Basciano, L.C., Peterson, R.C., 2007. Jarosite-hydronium jarosite solid-solution series with full iron site occupancy: mineralogy and crystal chemistry. Am. Mineral. 92, 1464–1473.

Beavis, S., Beavis, F., Somerville, P., Welch, S., 2005. Spatial and temporal variability of acidity at a coastal acid sulfate soil site II: a time for change. In: Roach, I.C. (Ed.), Regolith 2005—– Ten Years of CRC LEME. CRC LEME, pp. 22–26.

Becker, U., Gasharova, B., 2001. AFM observations and simulations of jarosite growth at the molecular scale: probing the basis for the incorporation of foreign ions into jarosite as a storage mineral. Phys. Chem. Minerals 28, 545–556.

Bethke, C.M., 2006. The Geochemist's Workbench®, Release 6.0, A Reference Manual. Hydrogeology Program, University of Illinois. 241 pp.

Bigham, J.M., Nordstrom, D.K., 2000. Iron and aluminum hydroxysulfates from acid sulfate waters. In: Alpers, C.N., Jambor, J.L., Nordstrom, D.K. (Eds.), Sulfate Minerals — Crystallography, Geochemistry and Environmental Significance. Reviews in Mineralogy & Geochemistry, 40, pp. 351–403.

Casey, W.H., Banfield, J.F., Westrich, H.R., McLaughlin, L., 1993. What do dissolution experiments tell us about natural weathering. Chem. Geol. 105, 1–15.

Dill, H.G., 2001. The geology of aluminium phosphates and sulphates of the alunite group minerals: a review. Earth-Science Reviews 53, 35–93.

Drouet, C., Navrotsky, A., 2003. Synthesis, characterization, and thermochemistry of K–Na–H_3O jarosites. Geochim. Cosmochim. Acta 67, 2063–2076.

Drouet, C., Pass, K.L., Baron, D., Draucker, S., Navrotsky, A., 2004. Thermochemistry of jarosite–alunite and natrojarosite–natroalunite solid solutions. Geochim. Cosmochim. Acta 68, 2197–2205.

Dutrizac, J.E., Jambor, J.L., 2000. Jarosites and their application in hydrometallurgy. In: Alpers, C.N., Jambor, J.L., Nordstrom, D.K. (Eds.), Sulfate Minerals — Crystallography, Geochemistry and Environmental Significance Reviews in Mineralogy & Geochemistry, 40, pp. 405–452.

Gaboreau, S., Viellard, P., 2004. Prediction of Gibbs free energies of formation of minerals of the alunite supergroup. Geochim. Cosmochim. Acta 68, 3307–3316.

Gore, D., Creagh, D.C., Burgess, J.S., Colhoun, E.A., Spate, A.P., Baird, A.S., 1996. Composition, distribution and origin of surficial salts in the Vestfold Hills, East Antarctica. Antarct. Sci. 8, 73–84.

Gasharova, B., Gottlicher, J., Becker, U., 2005. Dissolution at the surface of jarosite: an *in situ* AFM study. Chem. Geol. 215, 499–516.

Isaacson, L., Kirste, D., Beavis, S., Welch, S., 2006. Controls of acid, salt and metal distribution at a coastal acid sulfate soils site. Regolith 2006: consolidation and dispersion of ideas. In: Fitzpatrick, R.W., Shand, P. (Eds.), Proceedings of the CRC LEME Regolith Symposium, November 2006, pp. 166–170.

Jambor, J.I., Nordstrom, D.K., Alpers, C.N., 2000. Metal-sulfate salts from sulfide mineral oxidation. In: Alpers, C.N., Jambor, J.L., Nordstrom, D.K. (Eds.), Sulfate Minerals — Crystallography, Geochemistry and Environmental Significance Reviews in Mineralogy & Geochemistry, 40, pp. 303–350.

Klingelhöfer, G., Morris, R.V., Bernhardt, B., Schroder, C., Rodionov, D.S., de Souza, P.A., Yen, A., Gellert, R., Evlanov, E.N., Zubkov, B., Foh, J., Bonnes, U., Kankeleit, E., Gutlich, P., Ming, D.W., Renz, F., Wdowiak, T., Squyres, S.W., Arvidson, R.E., 2004. Jarosite and hematite at Meridiani Planum from Opportunity's Mössbauer spectrometer. Science 306, 1740–1745.

Kolitsch, U., Pring, A., 2001. Crystal chemistry of the crandallite, beudantite and alunite groups: a review and evaluation of the suitability as storage materials for toxic metals. J. Mineral. Petrol. Sci. 96, 67–78.

Langmuir, D. and Whittemore, D.O., 1971. Variations in the stability of precipitated ferric oxyhyroxides. In Nonequilibrium Systems in Natural Water Chemistry (ed. J.D. Hem); ACS Advances in Chemistry Series, No. 106, 209–234

Madden, M.E.E., Bodnar, R.J., Rimstidt, J.D., 2004. Jarosite as an indicator of water-limited chemical weathering on Mars. Nature 431, 821–823.

Majzlan, J., Navrotsky, A., Schwertmann, U., 2004. Thermodynamics of iron oxides: Part III. Enthalpies of formation and stability of ferrihydrite (~$Fe(OH)_3$), schwertmannite (~$FeO(OH)_{3/4}(SO_4)_{1/8}$, and ε-$Fe_2O_3$. Geochim. Cosmochim. Acta 68, 1049–1059.

Oelkers, E.H., Schott, J., Devidal, J.L., 1994. The effect of aluminum, pH, and chemical affinity on the rates of aluminosilicate dissolution reactions. Geochim. Cosmochim. Acta 58, 661–669.

Papike, J.J., Karner, J.M., Shearer, C.K., 2006a. Comparative planetary mineralogy: Implications of martian and terrestrial jarosite. A crystal chemical perspective. Geochim. Cosmochim. Acta 70, 1309–1321.

Papike, J.J., Karner, J.M., Spilde, M.N., Shearer, C.K., 2006b. Terrestrial analogs of martian sulfates: major and minor element systematics of alunite jarosite from Goldfield, Nevada. Am. Mineral. 91, 1197–1200.

Preda, M., Cox, M.E., 2004. Temporal variations of mineral character of acid-producing pyritic coastal sediments, Southeast Queensland, Australia. Sci. Total Environ. 326, 257–269.

Ralph, J. and Ralph, I. 1993. MINDAT database. http://www.mindat.org, cited in May 2007.

Santelli, C.M., Welch, S.A., Westrich, H.R., Banfield, J.F., 2001. Fe oxidizing bacteria and the weathering of Fe silicate minerals. Chem. Geol. 180, 99–115.

Sasaki, K., Konno, H., 2000. Morphology of jarosite-group compounds precipitated from biologically and chemically oxidized Fe ions. Canad. Mineral. 38, 45–56.

Singer, P.C., Stumm, W., 1970. Acidic mine drainage. rate-determining step. Science 167, 1121–1124.

Smith, A.M.L., Dubbin, W.E., Wright, K., Hudson-Edwards, K.A., 2006a. Dissolution of lead- and lead–arsenic–jarosites at pH 2 and 8 and 20 °C: insights from batch experiments. Chem. Geol. 229, 344–361.

Smith, A.M.L., Hudson-Edwards, K.A., Dubbin, W.E., Wright, K., 2006b. Defects and impurities in jarosite: a computer simulation study. Appl. Geochem. 21, 1251–1258.

Smith, A.M.L., Hudson-Edwards, K.A., Dubbin, W.E., Wright, K., 2006c. Dissolution of jarosite [$KFe_3(SO_4)_2(OH)_6$] at pH 2 and 8: Insights from batch experiments and computational modelling. Geochim. Cosmochim. Acta, 70, 608–621.

Somerville, P., Beavis, S., Welch, S., 2004. Spatial and temporal variability of acidity at a coastal acid sulfate soil site. In: Roach, I.C. (Ed.), Advances in Regolith. CRC LEME, pp. 335–339.
Stoffregen, R.E., 1993. Stability relations of jarosite and natrojarosite. Geochim. Cosmochim. Acta 57, 2417–2419.
Sullivan, L.A., Bush, R.T., 2004. Iron precipitate accumulations associated with waterways in drained coastal acid sulfate landscapes of eastern Australia. Mar. Freshw. Res. 55, 727–736.
Tulau, M.J., Naylor, S.D., 1999. Acid sulfate soil management priority areas in the lower Macleay floodplain. NSW Department of Land and Water Conservation.
Walker, P.H., 1972. Seasonal and stratigraphic controls in coastal floodplain soils. Aust. J. Soil Res 10, 127–142.
Velbel, M.A., 1993. Formation of protective surface layers during silicate-mineral weathering under well-leached, oxidizing conditions. Am. Mineral. 78, 405–414.
Welch, S.A., Ullman, W.J., 1993. The effect of organic acids on feldspar dissolution rates and stoichiometry. Geochim. Cosmochim. Acta 57, 2725–2736.
Welch, S.A., Christy, A.G., Kirste, D., Beavis, F.R., Beavis, S.B., 2007. Jarosite dissolution I-Trace cation flux in acid sulfate soils. Chem. Geol. 245, 183–197.
White, A.F., Brantley, S.L., 2003. The effect of time on the weathering of silicate minerals: why do weathering rates differ in the laboratory versus field. Chem. Geol. 202, 479–506.
White, I., Melville, M.D., Wilson, B.P., Sammut, J., 1997. Reducing acid discharges from coastal wetlands in eastern Australia. Wetlands Ecol. Manag. 5, 55–72.
Wogelius, R.A., Walther, J.V., 1992. Olivine dissolution kinetics at near-surface conditions. Chem. Geol. 97, 101–112.